Observation of acetyl phosphate formation in mammalian mitochondria using real-time in-organelle NMR metabolomics

Wen Jun Xu[a], He Wen[a,b], Han Sun Kim[a], Yoon-Joo Ko[c], Seung-Mo Dong[d], In-Sun Park[d], Jong In Yook[e], and Sunghyouk Park[a,1]

[a]Natural Product Research Institute, College of Pharmacy, Seoul National University, Gwanak-gu, 151-742 Seoul, Korea; [b]Department of Biochemistry and Molecular Biology, Shenzhen University School of Medicine, 518060 Shenzhen, China; [c]National Center for Inter-University Research Facilities, Seoul National University, Gwanak-gu, 151-742 Seoul, Korea; [d]Department of Anatomy, College of Medicine, Inha University, Nam-gu, 402-751 Incheon, Korea; and [e]Department of Oral Pathology, Oral Cancer Research Institute, College of Dentistry, Yonsei University, Seodaemun-gu, 120-752 Seoul, Korea

Edited by G. Marius Clore, National Institutes of Health, National Institute of Diabetes and Digestive and Kidney Diseases, Bethesda, MD, and approved March 12, 2018 (received for review December 7, 2017)

Recent studies point out the link between altered mitochondrial metabolism and cancer, and detailed understanding of mitochondrial metabolism requires real-time detection of its metabolites. Employing heteronuclear 2D NMR spectroscopy and $^{13}C_3$-pyruvate, we propose in-organelle metabolomics that allows for the monitoring of mitochondrial metabolic changes in real time. The approach identified acetyl phosphate from human mitochondria, whose production has been largely neglected in eukaryotic metabolism since its first description about 70 years ago in bacteria. The kinetic profile of acetyl phosphate formation was biphasic, and its transient nature suggested its role as a metabolic intermediate. The method also allowed for the estimation of pyruvate dehydrogenase (PDH) enzyme activity through monitoring of the acetyl-CoA formation, independent of competing cytosolic metabolism. The results confirmed the positive regulation of mitochondrial PDH activity by p53, a well-known tumor suppressor. Our approach can easily be applied to other organelle-specific metabolic studies.

real time | metabolomics | NMR | mitochondria | acetyl phosphate

Mitochondria are metabolic organelles that carry out fundamental functions of eukaryotic life. With the recognition of metabolic perturbations as hallmark characteristics of cancers (1, 2), mitochondrial metabolism has been implicated in tumorigenesis (3). As metabolism is essentially concerned with flux or time-dependent metabolite changes, mitochondrial metabolism is best studied by real-time detection of the metabolites using live (functional) mitochondria. However, most of the mitochondrial metabolic studies have used cell or mitochondrial lysates and measured metabolites at a fixed time point (4). Current approaches to metabolic flux measurement include complicated isotope pattern analysis or mathematical modeling (5), but they are indirect and require mitochondrial sample destruction. Although real-time metabolic measurements are possible with ^{13}C-hyperpolarized NMR (6) and one-dimensional ^{13}C NMR spectroscopy with isolated mitochondria (7), these methods suffer from extreme hardware requirements and disappointingly low sensitivity with signal overlap, respectively. Therefore, a simple and efficient technique to measure real-time metabolic activities from live mitochondria is highly desired.

Pyruvate is arguably the most important carbon source for the tricarboxylic acid (TCA) cycle, a characteristic mitochondrial metabolism. Pyruvate is converted to acetyl-CoA through pyruvate dehydrogenase (PDH), and the latter is condensed with oxaloacetate to form citrate, starting the first step of the TCA cycle. Acetyl-CoA is also a central metabolite in several metabolisms, such as fatty acid synthesis in cytosol and epigenetic modification in nuclei. Enzymes in mitochondrial pyruvate-related pathways, such as PDH and TCA cycle enzymes, have been importantly implicated in tumorigenesis (8, 9). Therefore, studying mitochondrial pyruvate metabolism with a real-time approach may lead to previously unseen metabolic activities involved in cancer-related mitochondrial metabolism.

Previously, we introduced in-cell live 2D NMR metabolomics for real-time metabolomic study at the whole-cell level (10). Here, carrying the concept to a higher tier for an organelle level, we sought to investigate the pyruvate metabolism of live mitochondria in real time using 2D in-organelle NMR metabolomics.

Results and Discussion

Integrity of Live Mitochondrial Samples. To implement the approach, we prepared pure mitochondria from a human colon cancer cell line (HCT116) with virtually no contamination from cytosol (Fig. 1*A*). HSP60, a mitochondrial marker, and GAPDH, a cytosolic marker, were shown to be absent in cytosolic and mitochondrial preparations, respectively. The absence of cytosolic contamination was further confirmed using NMR spectroscopy (see *NMR Experiments on Live Mitochondria and the Identification of Acetyl Phosphate*). We assured the physical and functional integrities of the prepared mitochondria, which can significantly affect the results, by using several test procedures.

Significance

We introduce an in-organelle live NMR metabolomics approach that allows for real-time metabolic monitoring of live human mitochondria. The approach also features more than an order of magnitude higher sensitivity and much less overlap than conventional methods. The real-time monitoring capability identified acetyl phosphate in human mitochondria and showed its biphasic kinetic profile typical of a reaction intermediate. The method also allowed for estimation of pyruvate dehydrogenase enzyme activity in live mitochondria according to p53 status, independent of competing cytosolic metabolism. Our approach should be very useful in studies on mitochondrial-specific contributions to cancer metabolism, and can be straightforwardly extended to studies on other diseases with altered mitochondrial metabolism.

Author contributions: S.P. designed research; W.J.X., H.W., H.S.K., Y.-J.K., S.-M.D., and I.-S.P. performed research; W.J.X., H.W., H.S.K., Y.-J.K., S.-M.D., I.-S.P., and J.I.Y. contributed new reagents/analytic tools; W.J.X., H.W., H.S.K., and S.P. analyzed data; and S.P. wrote the paper.

The authors declare no conflict of interest.

This article is a PNAS Direct Submission.

[1]To whom correspondence should be addressed. Email: psh@snu.ac.kr.

This article contains supporting information online at www.pnas.org/lookup/suppl/doi:10.1073/pnas.1720908115/-/DCSupplemental.

Published online April 2, 2018.

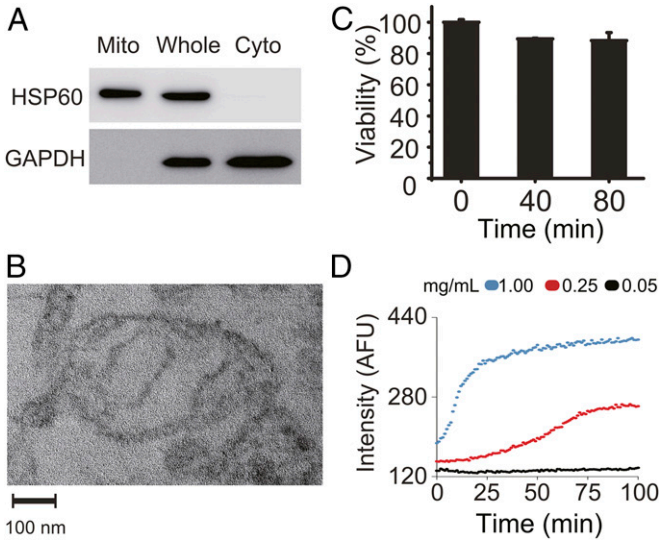

Fig. 1. Integrity and metabolic functionalities of live mitochondrial preparations. (*A*) Western blot for mitochondrial and cytosolic preparations. Mitochondrial marker (HSP60) and cytosolic marker (GAPDH) were probed in mitochondrial (Mito), whole-cell (Whole), and cytosolic (Cyto) preparations. (*B*) Transmission electron micrograph of isolated mitochondria. (*C*) MTT assay for mitochondrial samples. The mitochondria were incubated for the indicated periods in an NMR tube as in a real live NMR measurement, after which the MTT assay was performed. (*D*) Oxygen consumption of the mitochondrial samples obtained with the MitoXpress dye. Mitochondrial concentrations (as mitochondrial proteins): 0.05 mg/mL (black), 0.25 mg/mL (red), and 1 mg/mL (blue). AFU, arbitrary fluorescence unit.

First, the physical integrity of mitochondria was confirmed by observing intact mitochondria under an electron microscope (Fig. 1*B*). Second, the metabolic functionality of the mitochondria sampled from an NMR tube before, during, and after the NMR experiment was tested by 3-(4,5-dimethylthiazol-2-yl)-2,5-diphenyltetrazolium bromide (MTT) colorimetric assay that depends on mitochondrial redox enzymes (11). The results showed that the mitochondrial activities did not change much over the period of 80 min, the maximum decrease being only about 10% (Fig. 1*C*). Third, the oxygen consumption of the mitochondria was measured using the MitoXpress probe (Fig. 1*D*). The results showed that the oxygen in the mitochondrial sample was consumed over time in a mitochondrial amount-dependent manner up to 100 min. Overall, these results confirmed that the prepared mitochondria were metabolically functional and an appropriate system for real-time metabolomic assessment of live mitochondria.

NMR Experiments on Live Mitochondria and the Identification of Acetyl Phosphate. For actual NMR experiments, the mitochondrial preparations were directly placed into a 5-mm Shigemi NMR tube with $^{13}C_3$-labeled pyruvate (3 mM), and a total of eight ^{1}H-detected 2D heteronuclear single-quantum coherence (HSQC) NMR spectra were obtained (~5 min each; see *Materials and Methods*). This very short time resolution was possible thanks to more than an order of magnitude higher sensitivity (32× theoretical, excluding relaxation) of ^{1}H-detected HSQC than the previous ^{13}C-based 1D NMR spectroscopy approach for isolated mitochondria (7). The obtained spectra featured time-dependent peak changes for metabolites produced from pyruvate (Fig. 2*A*), confirming the functional mitochondrial activity. In comparison, none of these metabolites were observed without the addition of $^{13}C_3$-pyruvate (Fig. S1). The NMR data also allowed for the assurance of the absence of mitochondrial membrane leakage and cytosolic contamination. We performed the same NMR experiment with UK5099, a specific inhibitor of mitochondrial pyruvate carrier that blocks the transport of pyruvate across the mitochondrial membrane (12). UK5099 treatment blocked the generation of all of the observed metabolites as well as the consumption of pyruvate (Fig. 2*B*). Mitochondrial enzymes released from ruptured mitochondria or contaminating cytosolic enzymes would not be inhibited by the pyruvate transport inhibitor. Therefore, all of the observed metabolites in the original experiment must have been produced by mitochondrial enzymes in intact mitochondria. Most of the peaks on the spectra could be readily assigned based on the biochemical pathways for pyruvate metabolism and the chemical shifts of the standard compounds (Fig. 2*A* and Table S1). These metabolites

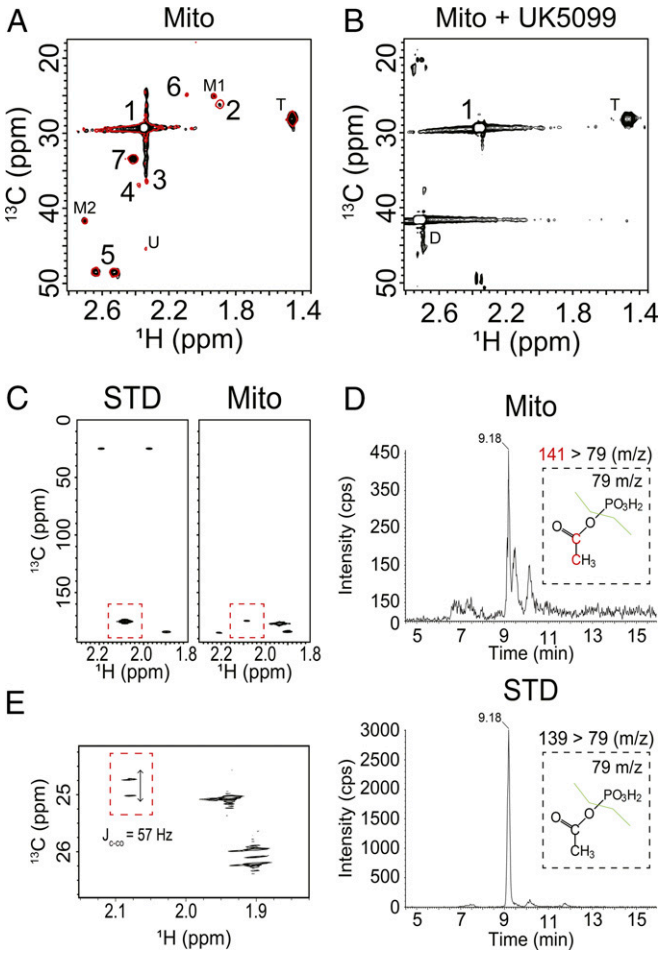

Fig. 2. HSQC spectra on live mitochondria and the identification of acetyl phosphate. (*A*) Overlaid spectra taken at 5 min (black) and 40 min (red) after the addition of $^{13}C_3$-pyruvate. (*B*) 2D HSQC spectrum of mitochondrial preparation at 40 min after the addition of $^{13}C_3$-pyruvate and UK5099 (3 mM). For *A* and *B*, mitochondrial samples corresponding to about 400 μg of mitochondrial protein were used. The numbers and symbols indicate assigned metabolites for *A* and *B*: 1, pyruvate; 2, acetate; 3, glutamate; 4, succinate; 5, citrate; 6, acetyl phosphate (tentative); 7, glutamine; T, the tautomer peak of pyruvate; M1 and M2, putative natural abundance mitochondrial peaks; U, unidentified peak; and D, DMSO (see Table S1). (*C*) 2D decoupled HMBC spectra for acetyl phosphate standard (STD) (*Left*), and a mitochondrial extract (Mito) (*Right*) (red boxes: ^{1}H = 2.09 ppm, ^{13}C = 175.2 ppm). (*D*) Multiple reaction monitoring detection of acetyl phosphate from a mitochondrial extract (Mito) (*Top*), and acetyl phosphate standard (STD) (*Bottom*) using LC-MS/MS. Red in *Top* indicates ^{13}C isotopes. (*E*) High-resolution 2D HSQC spectrum of mitochondrial samples with nonuniform sampling. The red box indicates the carbon–carbon *J*-splitting (57 Hz) of the methyl group of acetyl phosphate (^{1}H = 2.09 ppm, ^{13}C = 24.96 ppm).

BIOCHEMISTRY

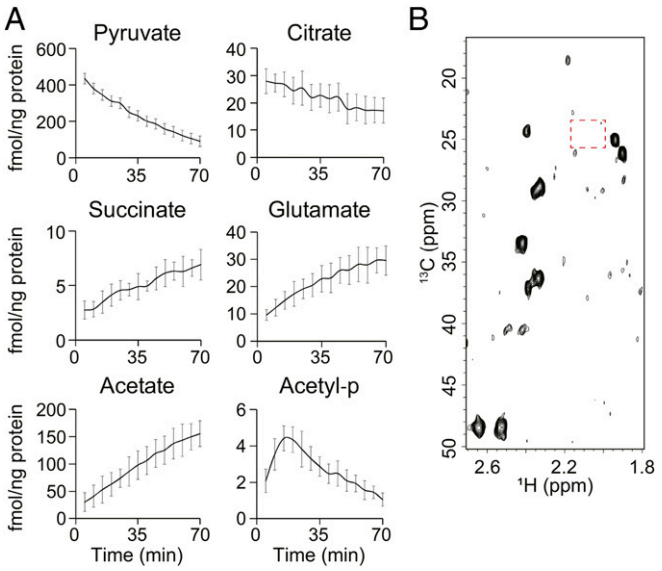

Fig. 3. Real-time measurements of metabolites from live mitochondria. (*A*) Time-resolved metabolite-level changes in live mitochondria. The data represent the average of six independent experiments (the overlays of all of these datasets are shown in Fig. S2). Error bars indicate the SD. The *y* axis represents femtomoles of metabolites divided by nanograms of mitochondrial protein. The metabolite amount was obtained in reference to the internal standard, TSP (1.45 mM), and each sample was normalized by the amount of mitochondrial protein (about 1.5 mg) obtained with BCA assay. Acetyl-p indicates acetyl phosphate. (*B*) An HSQC spectrum for a mitochondrial extract after 80 min incubation with $^{13}C_3$-pyruvate. The red box represents the position for acetyl phosphate (^{1}H = 2.09 ppm, ^{13}C = 24.96 ppm).

represent those formed before, during, and after the TCA cycle that can serve as specific probe metabolites for various metabolic nodes in mitochondria. Additionally, a peak at (^{1}H = 2.09 ppm, ^{13}C = 24.96 ppm) (peak 6 in Fig. 2*A*) was tentatively assigned as acetyl phosphate. Its formation from pyruvate has not been reported in human mitochondria, with reports only in bacteria (13). Given the well-known differences between bacterial and human metabolism, we pursued further confirmation of its identity. As we observed only one H–C correlation of the two carbon atoms of acetyl phosphate, we separately obtained the heteronuclear multiple-bond correlation (HMBC) spectrum for the other H–C–CO correlation. For this, much more mitochondrial extract was prepared separately, because the metabolite turned out to be quite labile (see *Biphasic Kinetic Profile of Acetyl Phosphate Metabolism*) and HMBC is less sensitive than HSQC. The H–C–CO correlation appeared exactly at the chemical shift of the standard compound (Fig. 2*C*). Further proof of the presence of acetyl phosphate came from the mass spectrometric analysis of the lysate sample, which showed the characteristic MS/MS peak by the loss of H_2PO_3 from the acetyl phosphate molecular ion (Fig. 2*D*). The increase in the *m*/*z* value of the molecular ion compared with the database value (from *m*/*z* 139 to 141) showed its formation from the added $^{13}C_3$-pyruvate. This was also confirmed by J_{C-CO} splitting (57 Hz) of the methyl group in the high-resolution nonuniformly sampled HSQC (Fig. 2*E*) (14). Therefore, the NMR and mass spectrometry results prove the synthesis of acetyl phosphate from pyruvate in human mitochondria. It is also worth noting that the discovery of pyruvate-to-acetyl phosphate conversion in bacteria (15, 16) was a milestone for the later discoveries of CoA and acetyl-CoA in eukaryotes (17, 18), which resulted in two Nobel prizes to Lipmann (1953) and Lynen (1964). Lipmann's work showed that acetyl phosphate is an intermediate for the phosphorylation of adenylate by pyruvate dehydrogenation in both aerobic and anaerobic conditions with bacterial lysates. However, as acetyl-CoA was considered the primary carrier of a high-energy acetyl group, the presence and roles of acetyl phosphate in animals have been largely neglected for more than 70 years, with very few studies reporting its formation from citrate in the 1960s (19). In those studies, it was suggested that acetyl phosphate might be involved in acetylation and ketone body formation through an acetyl-CoA intermediate in the absence of ATP. Our identification and these previous studies may point to a previously uncharacterized metabolic pathway in human mitochondria, possibly involved in phosphorylation or acetylation.

Biphasic Kinetic Profile of Acetyl Phosphate Metabolism. As the metabolism of acetyl phosphate in human mitochondria has not been established, we took advantage of the real-time monitoring of our approach and followed the time course of its formation. Very interestingly, acetyl phosphate exhibited a biphasic time profile, with a decrease in its level after an initial rapid increase for about 15 min (Fig. 3*A*). In addition, it could not be detected in the mitochondrial lysate obtained after a long incubation time (~80 min), suggesting its rather rapid degradation (Fig. 3*B*). This easy degradability and relatively low concentration may explain why acetyl phosphate has not been described in human mitochondria so far. It is also consistent with rather rapid degradation of synthetic acetyl phosphate in animal tissue lysates (17). In comparison, the levels of acetate, succinate, and glutamate steadily increased over the entire experimental time, while that of citrate decreased. In a kinetic perspective, these time courses actually resemble the product and intermediate formations in a steady-state reaction profile. Because hydrolysis of the high-energy phosphoester bond in acetyl phosphate can lead to acetate formation, it might be suggested that acetyl phosphate is an intermediate of acetate formation in mitochondria, although this may not be the major pathway. Consistently, an acylphosphatase (EC 3.6.1.7) that can hydrolyze an acyl phosphoester bond has been reported in the human genome (20). The confirmation of this acetate formation from an acetyl phosphate intermediate requires thorough biological studies, which may also confirm a new mitochondrial metabolic pathway. The steady decrease of citrate and increases of succinate and glutamate seem also consistent with known metabolic pathways. As citrate is an early intermediate for succinate and glutamate synthesis from pyruvate, its level may decrease steadily while those of the two products increase in the experimental time frame. Before this decrease, however, there must have been an initial increase in citrate that could not be measured due to the experimental dead time (~5 min), as citrate was not detected at time 0 (before pyruvate addition; Fig. S1).

Real-Time Monitoring of Acetyl-CoA Formation Through PDH and the Effects of p53. Another critical metabolite produced from pyruvate is acetyl-CoA. Despite its metabolic importance, measuring acetyl-CoA formation through a specific pathway has been very challenging because it is metabolized through several pathways in different cellular compartments (i.e., mitochondria, cytosol, and nucleus). As PDH is a mitochondrial enzyme and uses pyruvate as a substrate, our approach should be relevant for direct assessment of acetyl-CoA production via the PDH-mediated pathway. To measure acetyl-CoA production, we added CoA, because acetyl-CoA formation through PDH requires a quantitative amount of CoA (Fig. 4*A*). The acetyl-CoA peak was observed in this condition, and UK5099 blocked its formation (Fig. 4*B*). These results show that our approach specifically detected mitochondrial PDH-mediated acetyl-CoA formation, independent of other competing pathways. Next, to evaluate the PDH enzyme activity in live mitochondria, we measured the acetyl-CoA formation in real time. Particularly, we used mitochondria from HCT116 cells with p53 wild-type (WT) or knockout (KO) status (Fig. 4*C*). p53 is one of the most frequently mutated genes in

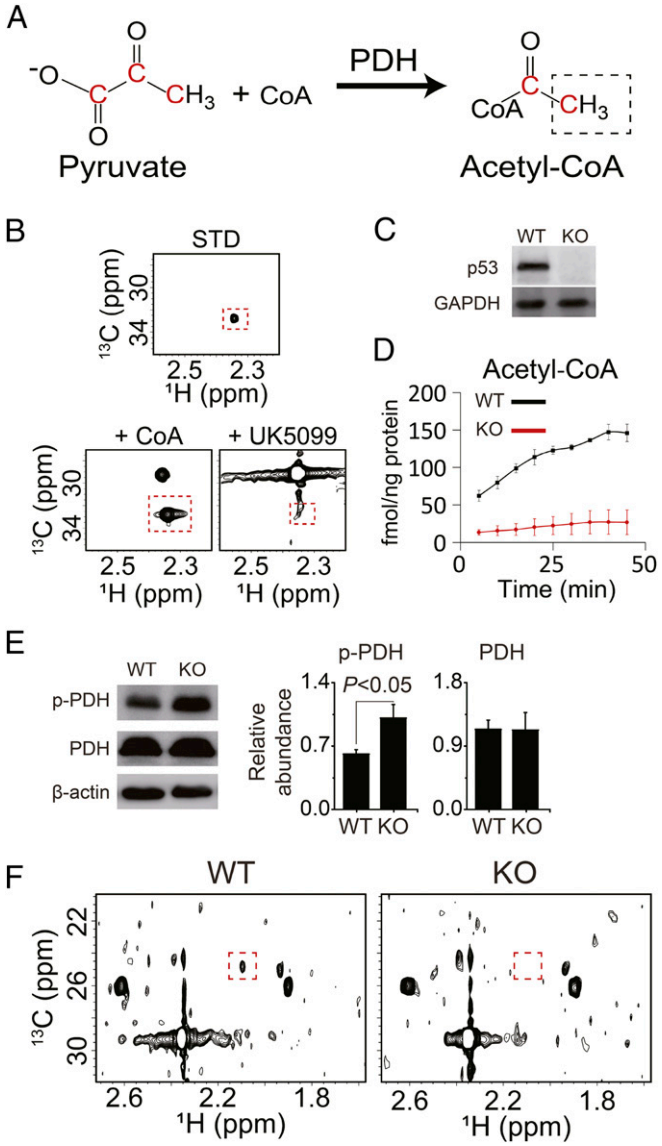

Fig. 4. Measurement of acetyl-CoA production in live mitochondria. (*A*) Conversion of $^{13}C_3$-pyruvate into $^{13}C_2$-acetyl-CoA by PDH. Red indicates ^{13}C isotopes. (*B*) HSQC spectra of standard acetyl-CoA (STD) (*Top*), mitochondrial preparations 40 min after the addition of $^{13}C_3$-pyruvate and CoA (*Bottom Left*), and the same experiment with added UK5099 (*Bottom Right*). The red boxes correspond to the methyl peak of acetyl-CoA (^1H = 2.34 ppm, ^{13}C = 32.76 ppm). (*C*) Western blot of the HCT116 WT and KO cells for p53. (*D*) Time-resolved acetyl-CoA changes in live mitochondria from p53 WT (black) and p53 KO (red) cells. The data represent the average of three independent experiments. Error bars indicate the SD. The *y* axis represents femtomoles of metabolites divided by nanograms of mitochondrial protein. (*E*) Western blot (*Left*) for PDH, p-PDH, and β-actin. The bar charts (*Right*) represent the relative amounts of the respective enzymes normalized to that of β-actin (n = 3). A significant change is indicated as $P < 0.05$ by Student's t test. The error bars indicate the SD. (*F*) HSQC spectra of live mitochondrial preparations of p53 WT and KO cells taken at 30 min after the addition of $^{13}C_3$-pyruvate and CoA. The red boxes correspond to the methyl peak of acetyl phosphate (^1H = 2.09 ppm, ^{13}C = 24.96 ppm). For *B*, *D*, and *F*, mitochondrial samples corresponding to about 400 μg of mitochondrial protein were used.

cancer (21) and can profoundly modulate pyruvate metabolism (22). We observed a significantly higher rate of acetyl-CoA formation from the mitochondria of the p53 WT cells (Fig. 4*D*), suggesting that p53 up-regulates the PDH activity. The PDH activity was also assessed through biological methods by the levels of PDH and phosphorylated PDH (p-PDH), an inactive form of PDH. The Western blot data showed lower levels of the inactive p-PDH in WT cells without the changes in total PDH (Fig. 4*E*), suggesting that the elevated acetyl-CoA formation reflects the higher activity of PDH in WT cells. Our data confirm previous suggestions that p53 modulates the PDH activity through the regulation of PDH kinase, which phosphorylates PDH (23). Another interesting finding from using p53 WT/KO cells is the dependence of acetyl phosphate formation on p53 status: the acetyl phosphate peak was observed only in the presence of WT p53 (Fig. 4*F*). This suggests that acetyl phosphate may have implications for cancer mitochondrial metabolism, given the roles of p53 in cancer. Pyruvate metabolism to lactate in cytosol is enhanced (Warburg effect), while its metabolism by PDH in mitochondria is compromised in many cancer cells with p53 mutations (23, 24). Because our results show higher formation of acetyl phosphate and acetyl-CoA along with enhanced PDH activity in p53 WT cells, the regulation of these two molecules may be associated with p53's tumor suppressor activity through PDH modulation and Warburg effect suppression.

In conclusion, our in-organelle live 2D NMR metabolomics approach, with its high sensitivity and time-resolved monitoring, enabled the observation of previously uncharacterized acetyl phosphate in human mitochondria. In addition, it allowed for the measurement of mitochondrial PDH-specific production of acetyl-CoA, as modulated by p53. The approach should allow for detailed understanding of mitochondrial cancer metabolism, independent of competing cytosolic pathways. Recently, mitochondrial malfunction has been implicated in the pathophysiologies of other diseases such as Alzheimer's, Parkinson's, and muscular dystrophy, and therapeutic approaches targeting mitochondria are being explored (25–27). Therefore, our method could also be applied to both basic mechanisms and novel therapeutics for those diseases.

Materials and Methods

Chemicals and Reagents. UK5099, a specific inhibitor of the mitochondrial pyruvate carrier, was purchased from Santa Cruz Biotechnology. The stable isotope-labeled $^{13}C_3$-pyruvate (99%) and sodium 3-(trimethylsilyl)propionate (2,2,3,3-d_4) (TSP) (98% purity) were purchased from Cambridge Isotope Laboratories. Other chemicals, including malate, ADP, NAD, ATP, acetyl-CoA, CoA, glutamate, acetate, glutamine, citrate, and acetyl phosphate, were obtained from Sigma-Aldrich.

Cell Lines. Both HCT116 WT and KO cells were cultured in DMEM (Biowest) supplemented with 10% heat-inactivated FBS (Biowest) and 100 U/mL penicillin-streptomycin (HyClone) at 37 °C in a 5% CO_2 humidified incubator.

Mitochondrial Isolation and Sample Preparation for Live Mitochondrial NMR Metabolomics. Mitochondria were isolated from 1×10^8 HCT116 cells using a mitochondria isolation kit (Qiagen) according to the manufacturer's instructions. The final mitochondrial pellet was washed with 1 mL of Dulbecco's phosphate-buffered saline (DPBS) by centrifugation. Small aliquots of samples were also taken for protein quantification with a bicinchoninic acid (BCA) protein assay kit (Thermo Fisher Scientific) and Western blot analysis. Mitochondria were resuspended in 100 μL of analysis buffer (120 mM KCl, 5 mM KH_2PO_4, 1 mM EGTA, and 3 mM Hepes pH 7.4) (28) and incubated for 30 min at 37 °C. Next, the mitochondrial preparation was mixed with 200 μL of pyruvate solution ($^{13}C_3$-pyruvate, malate, NAD, and ADP; pH 6.8). CoA was added as needed. The final concentrations were as follows: 0.25 mM malate, 0.25 mM NAD, 0.1 mM ADP, 3 mM CoA, and 3 mM $^{13}C_3$-pyruvate. D_2O (10%) for the lock purpose and TSP (1.45 mM) as an internal standard were also added. The mixture was then put in a 5-mm Shigemi tube for NMR analysis. For the treatment with UK5099, the concentration of UK5099 was 3 mM in the analysis buffer.

Mitochondrial MTT Assay. The functionality of the mitochondria during and after the NMR experiments was tested by MTT assay. A mitochondrial preparation was put into an NMR tube, and aliquots were taken out at 0-, 40-, and 80-min time points. Next, 8-μL mitochondrial suspensions were seeded on a 96-well plate containing 62 μL of NMR sample buffer (analysis buffer plus

pyruvate solution), 10 μL of MTT assay buffer (100 mM $MgCl_2$, 100 mM ATP, and 100 mM sodium succinate), and 20 μL of MTT solution (5 mg/mL). For each time point, the suspensions were transferred into 1.5 mL tubes and harvested by centrifugation. The formazan crystals in the suspensions were extracted with 100 μL of dimethyl sulfoxide (DMSO) and transferred to a 96-well plate for spectrophotometric quantitation at 595 nm using a microplate reader (VersaMax).

Mitochondrial Respiration Measurement. To confirm the functionality of the isolated mitochondria, respiration measurement was carried out with MitoXpress (Luxcel Biosciences) fluorescent dye following the manufacturer's protocol. The procedure involves a step that blocks oxygen exchange into the mitochondrial sample with mineral oil. The experiment was carried out with varying concentrations of mitochondria in 96-well plates. The fluorescence signal was measured at 1-min intervals for 100 min on a SpectraMax M5 microplate reader (Molecular Devices), with wavelengths of 380 nm for excitation and 650 nm for emission.

Sample Extraction for NMR Spectroscopy and LC-MS. Metabolite extraction was performed on isolated mitochondria from HCT116 cells. The metabolites were extracted using methanol, followed by freeze-drying. Methanol (1 mL) was added to the mitochondrial NMR sample (270 μL) for protein precipitation, and 6 mL of distilled water was also added for freeze-drying. Lastly, the freeze-dried pellet was resuspended in 270 μL of buffer composed of 2 mM Na_2HPO_4 and 5 mM NaH_2PO_4 in D_2O with TSP (1.45 mM) as an internal standard for NMR spectroscopy. After the NMR analysis, 10 μL of the NMR sample was mixed with 10 μL of acetonitrile, and 2 μL of the mixture was injected for LC-MS/MS analysis.

NMR Measurement. ^1H and ^{13}C HSQC NMR spectra were measured on a 600-MHz Bruker Avance spectrometer equipped with a cryogenic triple-resonance probe (National Center for Inter-University Research Facilities, Seoul National University). HSQC NMR spectra were acquired at 37 °C for the required time points, with the following parameters: pulse program, "hsqcetgpsisp2.2"; spectral widths, 80 ppm along the ^{13}C and 12 ppm along the ^1H dimensions; and 1,024 (for proton) × 128 (for carbon) points. One experiment took about 5 min. The decoupled HMBC spectrum was acquired using an HMQC pulse sequence (hmqcgpqf) with the heteronuclear *J* coupling parameter set to 7 Hz. The other parameters were the same as in a standard HMBC experiment.

Identification and Quantification of Metabolites. The metabolites were initially identified in reference to known pyruvate metabolic pathways and NMR metabolite databases such as the Human Metabolome Database (29), BioMagResBank (30), and SpinAssign (31). The identifications were further confirmed by spiking experiments with standard samples. For acetyl phosphate, additional confirmation was obtained using HMBC NMR spectroscopy and LC-MS. For quantification, we performed 2D integration of the metabolite peaks derived from $^{13}C_3$-pyruvate, as not all of the carbons can be from pyruvate. The particular proton–carbon pairs that were used for the peak quantifications are listed in Table S1. The levels of metabolites were expressed as amount of metabolites (in femtomoles) obtained from peak integrals, normalized by the amount of mitochondrial protein (in nanograms). The concentration of each metabolite was obtained using the internal standard (TSP, 1.45 mM) as the reference. Taking into account the natural abundance of the TSP signal and the number of protons, the amount of each metabolite in the total incubation volume of 270 μL was calculated. The mitochondrial protein amount was obtained using the well-established BCA assay procedure after dissolving the mitochondria in lysis buffer.

LC-MS/MS for Acetyl Phosphate Identification. For LC-MS/MS analysis, HPLC was performed on an Agilent 1100 Series liquid chromatography system (Agilent) with a ZIC-pHILIC polymeric bead, poly(ether-ether-ketone) (PEEK)-coated column (150 × 2.1 mm, 5 μm; Merck KGaA) at 35 °C. For the mobile phase, A and B were distilled water plus 10 mM ammonium carbonate (pH 9.0) and acetonitrile, respectively. The linear gradient was as follows: 80% B at 0 min, 35% B at 10 min, 5% B at 12 min, 5% B at 25 min, 80% B at 25.1 min, and 80% B at 35 min, with a 0.15 mL/min flow rate. MS data were acquired using an API 2000 mass spectrometer (AB/SCIEX) equipped with an electrospray ionization source. In detecting acetyl phosphate, the multiple reaction monitoring transitions of parent ion to fragment ion, 139>79 *m/z* for ^{12}C-acetyl phosphate and 141>79 *m/z* for $^{13}C_2$-acetyl phosphate, were monitored in a negative-ion detection mode.

Western Blot Analysis. Western blots were performed using a routine procedure with nitrocellulose membranes (Millipore). For detection, the following antibodies were used: rabbit polyclonal antibody against phospho-PDHE1-α Ser^{293} (EMD Millipore); mouse monoclonal antibodies against p53, PDHE1-α, HSP60, and β-actin; goat polyclonal antibodies against GAPDH; and horseradish peroxidase-conjugated secondary antibodies (Santa Cruz Biotechnology).

Transmission Electron Microscopy Analysis. The mitochondrial pellet isolated from 2×10^8 cells was fixed in 1% glutaraldehyde with 100 mM phosphate buffer for 2 h and washed with 100 mM phosphate buffer three times. After postfixation in 1% (wt/vol) osmium tetroxide (OsO4), the sample was dehydrated in increasing concentrations of ethanol (70%, 80%, 90%, 95%, and 100%) and immersed in propylene oxide as a transition solvent. Next, the sample was embedded in epon812 resin (Electron Microscopy Sciences) and polymerized at 60 °C for 73 h. After resin-embedding, the sample was cut into 60-nm thick sections with an ultramicrotome (Ultracut E; Reichert-Jung), and the sections were placed onto a 200-mesh copper grid (Electron Microscopy Sciences). The grid containing the sections was then stained in 3% uranyl acetate and lead citrate. After drying the grid, the sections were observed with a transmission electron microscope (JEM-1011; JEOL) operating at 80 kV.

ACKNOWLEDGMENTS. The research was supported by grants to S.P. from the Basic Science Research Program through the National Research Foundation of Korea funded by the Ministry of Education, Science, and Technology (2014-069340 and 2009-83533); the National R&D Program for Cancer Control (1420290); and the Bio-Synergy Research Project (NRF-2015M3A9C4075818) of the Ministry of Science, Information and Communication Technology, and Future Planning through the National Research Foundation of Korea.

1. Pavlova NN, Thompson CB (2016) The emerging hallmarks of cancer metabolism. *Cell Metab* 23:27–47.
2. Dang CV (2012) Links between metabolism and cancer. *Genes Dev* 26:877–890.
3. Zong WX, Rabinowitz JD, White E (2016) Mitochondria and Cancer. *Mol Cell* 61:667–676.
4. Demine S, Reddy N, Renard P, Raes M, Arnould T (2014) Unraveling biochemical pathways affected by mitochondrial dysfunctions using metabolomic approaches. *Metabolites* 4:831–878.
5. MacRae JI, et al. (2013) Mitochondrial metabolism of sexual and asexual blood stages of the malaria parasite *Plasmodium falciparum*. *BMC Biol* 11:67.
6. Park JM, et al. (2013) Measuring mitochondrial metabolism in rat brain in vivo using MR Spectroscopy of hyperpolarized [2-^{13}C]pyruvate. *NMR Biomed* 26:1197–1203.
7. Perrin A, Gout E, Chambaz EM, Defaye G (1994) Metabolism of malate in bovine adrenocortical mitochondria studied by ^{13}C-NMR spectroscopy. *Eur J Biochem* 223:51–59.
8. Gottlieb E, Tomlinson IP (2005) Mitochondrial tumour suppressors: a genetic and biochemical update. *Nat Rev Cancer* 5:857–866.
9. Chu QS, et al. (2015) A phase I open-labeled, single-arm, dose-escalation, study of dichloroacetate (DCA) in patients with advanced solid tumors. *Invest New Drugs* 33:603–610.
10. Wen H, An YJ, Xu WJ, Kang KW, Park S (2015) Real-time monitoring of cancer cell metabolism and effects of an anticancer agent using 2D in-cell NMR spectroscopy. *Angew Chem Int Ed Engl* 54:5374–5377.
11. Slater TF, Sawyer B, Straeuli U (1963) Studies on succinate-tetrazolium reductase systems: III. Points of coupling of four different tetrazolium salts. *Biochim Biophys Acta* 77:383–393.
12. Wiemer EA, Michels PA, Opperdoes FR (1995) The inhibition of pyruvate transport across the plasma membrane of the bloodstream form of *Trypanosoma brucei* and its metabolic implications. *Biochem J* 312:479–484.
13. Lipmann F (1944) Enzymatic synthesis of acetyl phosphate. *J Biol Chem* 155:55–70.
14. Lee S, et al. (2017) Carbon isotopomer analysis with non-unifom sampling HSQC NMR for cell extract and live cell metabolomics studies. *Anal Chem* 89:1078–1085.
15. Lipmann F (1939) Role of phosphate in pyruvic acid dehydrogenation. *Nature* 144: 381–382.
16. Lipmann F (1940) A phosphorylated oxidation product of pyruvic acid. *J Biol Chem* 134:463–464.
17. Lipmann F (1945) Acetylation of sulfanilamide by liver homogenates and extracts. *J Biol Chem* 160:173–190.
18. Lynen F, Reichert E (1951) Zur chemischen Struktur der "aktivierten Essigsäure" [The chemical structure of activated acetic acid]. *Angew Chem* 63:47–48.
19. Guly MF, Pechenova TN, Matusevich LI (1966) Pathway and enzymes of conversion of citric acid into acetyl phosphate in animal tissues. *Nature* 212:36–37.
20. Fiaschi T, et al. (1995) Cloning and expression of the cDNA coding for the erythrocyte isoenzyme of human acylphosphatase. *FEBS Lett* 367:145–148.
21. Levine AJ, Oren M (2009) The first 30 years of p53: growing ever more complex. *Nat Rev Cancer* 9:749–758.
22. Liu J, Zhang C, Hu W, Feng Z (2015) Tumor suppressor p53 and its mutants in cancer metabolism. *Cancer Lett* 356:197–203.

23. Contractor T, Harris CR (2012) p53 negatively regulates transcription of the pyruvate dehydrogenase kinase Pdk2. *Cancer Res* 72:560–567.
24. Allison SJ, et al. (2014) Identification of LDH-A as a therapeutic target for cancer cell killing via (i) p53/NAD(H)-dependent and (ii) p53-independent pathways. *Oncogenesis* 3:e102.
25. Vila MC, et al. (2017) Mitochondria mediate cell membrane repair and contribute to Duchenne muscular dystrophy. *Cell Death Differ* 24:330–342.
26. Fernández-Moriano C, González-Burgos E, Gómez-Serranillos MP (2015) Mitochondria-targeted protective compounds in Parkinson's and Alzheimer's diseases. *Oxid Med Cell Longev* 2015:408927.
27. Onyango IG, Khan SM, Bennett JP, Jr (2017) Mitochondria in the pathophysiology of Alzheimer's and Parkinson's diseases. *Front Biosci (Landmark Ed)* 22:854–872.
28. Bricker DK, et al. (2012) A mitochondrial pyruvate carrier required for pyruvate uptake in yeast, Drosophila, and humans. *Science* 337:96–100.
29. Wishart DS, et al. (2018) HMDB 4.0: the human metabolome database for 2018. *Nucleic Acids Res* 46:D608–D617.
30. Ulrich EL, et al. (2007) BioMagResBank. *Nucleic Acids Res* 36(Suppl 1):D402–D408.
31. Chikayama E, et al. (2010) Statistical indices for simultaneous large-scale metabolite detections for a single NMR spectrum. *Anal Chem* 82:1653–1658.